2020 IEEE/RSJ International Conference on Intelligent Robots and Systems (IROS)
October 25-29, 2020, Las Vegas, NV, USA (Virtual)

Magnetized Cell-robot Propelled by Magnetic Field for Cancer Killing

Yuguo Dai, Yanmin Feng, Lin Feng *,Yuanyuan Chen, Xue Bai, Shuzhang Liang, Li Song and Fumihito Arai

***Abstract*—In this paper, we present a magnetized cell-robot using macrophages as templates, which can be controlled under a strong gradient magnetic field, to approach and kill cancer cells in both vitro and vivo environment. Firstly, we establish a magnetic control system using only four coils which can generate gradient field up to 4.14 T/m utilizing the coupled field contributed by multiple electromagnets acting in concert. Most importantly, the cell-robot which is based on the macrophage is proposed, and can be transported to the vicinity of cancer cells precisely using strong gradient magnetic field. Then the cell-robot will actively phagocytose the cancer cells and eventually kill them, achieving the cancer treatment at the cellular level. It has important significance for guiding accurate targeted therapy in vivo for the future, under the premise of zero harm to the human body.**

I. Introduction

Realizing the three dimensional (3D) movement of a robot in complicated environments using non-contact methods, will considerably extend the operating scope compared with traditional methods[1-4]. Among the driving methods, the magnetic actuating technique is particularly promising, because it can be precisely controlled in 3D space[5-7] [8]. Also, the magnetic field will apply a force or a torque to any magnetic substance in the magnetic field, and a variety of robots have been fabricated and propelled by magnetic field[9-11]. This control method is especially promising for robots whose overall dimensions are millimeters, micrometers or even smaller, since at this scale the control accuracy and operation ability of the robot are greatly enhanced and it can be widely used in biomedicine, microfluidics[12, 13], and cell monitoring, which is very promising.

A magnetic device which convert magnetic energies into kinetic movement will overcome viscous resistance and realize the specifically adjustment of its posture, speed and direction[14]. Robotics offer the potential to improve the precision and safety of human surgery. With the goal of enabling less invasive and safer human surgery, as well as providing an increased level of dexterity desired by clinicians, the task of designing a system for magnetic manipulation of a fully untethered dexterous microrobotic device was undertaken. For example, the uniform field generated by the Helmholtz coil has the advantages of high uniformity and can response quickly[2, 15], and magnetic field at different directions can be obtained, but the magnetic flux density is generally small. Another example is the OctoMag system which can perform surgery inside the eyes[16]. The number of coils for a magnetic system has proved to be at least four to generate gradient force to realize 3D movement of a magnetic substance[17]. Therefore, for complex control of robot, a system with at least four coils is required.

Magnetic manipulation has emerged as a promising method in this regard because magnetic fields are capable of penetrating most materials with minimal interaction, and are nearly harmless to human beings[18]. Magnetic fields have been successfully used to wirelessly manipulate microdevices of various sizes and shapes[18]. Several magnetic propelled microrobots have been designed to carry drugs or do some test in vivo[19, 20]. However, challenges still exist, for example biocompatible and degradation problems haven't be solved yet. For medical robot, lots of study have been made towards cancer killing, drug delivery, or stem cell transplantation, and show great value. For example, the magnetic microrobot for carrying and delivering targeted cells[20], the swarm micropropellers penetrating the vitreous body of the eye[21], the spirulina magnetic microrobots for drug delivery to kill cancer cells[15], have shown great medical applications. Also, robots containing magnetic particles for cancer treatment or other medical usage, have been verified to be effective[22, 23]. Also, the immune cells, especially the macrophage have a variety property such as tumor targeting, preventing the spread of therapeutic agents into normal tissues[24]. Besides, using magnetic field propelled macrophage for tumor therapy has tested to be impressive[25], however the control part to realize 3D movement needs further improvement, since the tumor may locate at complex environment. Still, the macrophage can also act as drug carrier or something like that.

*Research supported by the Natural Science Foundation of Beijing (No.17L20128) and the National Key R&D Program of China (No. 2019YFB1309702)

Yuguo Dai (e-mail: daiyuguo5612@163.com), Xue Bai (e-mail: baixue041104@163.com), Li Song (e-mail: songlidjk@buaa.edu.cn), Shuzhang Liang (e-mail: liangsz13nq@buaa.edu.cn), are with Beihang University; School of Mechanical Engineering & Automation, Beijing, China.

Lin FENG (e-mail: linfeng@buaa.edu.cn), Yanmin Feng (e-mail: fengyanmin@buaa.edu.cn), Yuanyuan Chen (e-mail: chenyuanyuan0526@sina.com) are with Beihang University; School of Mechanical Engineering & Automation, and also with Beijing Advanced Innovation Center for Biomedical Engineering, Beihang University, Beijing 100083, China, (e-mail: linfeng@buaa.edu.cn).

Fumihito Arai (e-mail: arai@mech.nagoya-u.ac.jp), is with Department of Micro-Nano System Engineering, Nagoya University, Furo-cho, Chikusa-ku, Nagoya, 464-8603, Japan.

In this paper, we have designed a magnetic system that produces a large gradient magnetic field in the 3D space (more than 4.14 T/m), providing a solution for practical bioengineering applications. Then, we fabricated the cell-robot based on the mouse's macrophages while preserving the cell's viability. By putting the macrophage in the culture solution with nano magnetic particles and culturing the cells for a period, a magnetized cell-robot is obtained. Complex path control of the cell-robot is achieved using the gradient magnetic field and the cell-robot are also propelled by the field to approach the cancer cells in vitro which has promising applications for precise target treatment. Since macrophages can phagocytose foreign bodies[25, 26], the cell-robots can phagocytose cancer cells once they find the cancer cells, as a result killing them achieving immunotherapy. This would be instructive in achieving cell-level treatment in the future.

II. Experiment Setup

A. System setup

The established magnetic control system for propelling the cell-robot is shown in Fig. 1, which consists of four electromagnets and part of the work and the design of the system has been previously reported in [27]. The center of the four electromagnets is a spherical working area with a diameter of 90 mm. The system includes the computer control part, a magnetic field generating device, and the CCD cameras (HT2000CN) which can conduct the position tracking of the cell-robot. Wherein the number of turns of the coils and the diameter of each electromagnet are the same, parameters for each of the electromagnets are provided in Table I.

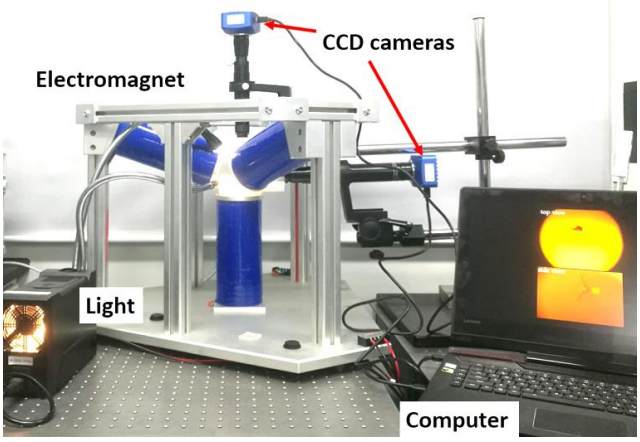

Fig. 1. Diagram of the electromagnet system, including the magnetic field generation part, the computer controlling part, and the image acquisition part.

TABLE I. ELECTROMAGNET PROPERTIES

Description	Value	Units
Number of Turns	914	---
Distance from Center	0.045	*m*
Diameter of Wire	2.24	*mm*
Coil Resistance	1.0	Ω
Core Inner Diameter	0.055	*m*
Core Outer Diameter	0.090	*m*
Coil Length	0.220	*m*

B. Magnetic field and simulation

In the vacuum environment, the magnetic field generated by a constant current element is only related to the magnitude of the current in the coil. The magnetic flux density can be calculated as:

$$d\boldsymbol{B} = \frac{\mu_0}{4\pi}\frac{Idl \times e_r}{\boldsymbol{r}^2} \quad (1)$$

Where Idl represents a constant-current source, $\boldsymbol{r}$ represents a radial vector pointing from a current element to the point P, $\mu_0 = 4\pi \times 10^{-7} N/A^2$, indicating the magnetic permeability in the vacuum environment. When the current source is loop-integrated, the magnetic field of a loop coil on its axis can be obtained:

$$\boldsymbol{B} = \frac{\mu_0 I R^2}{2(R^2+\boldsymbol{x}^2)^{3/2}} \quad (2)$$

Where R is the radius of the coil and $\boldsymbol{x}$ is the distance from a point on the axis to the center of the coil.

The core greatly enhances the intensity of the magnetic field, which leads to the magnetic field to be several or even tens times stronger compared without cores. However, the iron core usually has hysteresis effect which makes the magnetic field has no linear relationship with the magnitude of the current. This makes the control complicated. But for soft magnetic materials, the situation is different. For some soft magnetic materials like iron, the hysteresis is negligible within a certain range. In the newly established system, when an electromagnet is energized, the magnetic field generated by it will magnetize the cores of the remaining electromagnets, so that the size and distribution of the magnetic field will change. As shown in Fig. 2(a), we simulated the magnetic field at a specific position within the working area. Fig. 2(b) illustrates the magnetic distribution when only one coil G is working (I_G= 15A, I_D= I_E= I_F= 0A), while Fig. 2(c) shows the electromagnets working together (I_G= 15A, I_D= I_E= I_F= -15A). Since the maximum current in the coils is limited within 15A for safety, this helped generate a larger gradient field while the current in the coils is within the working rang.

Obviously, the magnetic field gradient is significantly enhanced by making the electromagnets work together and the gradient field at the working position is enhanced up to 4.14 T/m and quite uniform in the central area. Measurement along the Z-axis in the central working area under this condition (I_G= 15A, I_D= I_E= I_F= -15A) revealed a magnetic field that was consistent with the simulation results, with an intensity of up to 4.14 T/m and a high gradient field uniformity as shown in Fig. 2(d). Due to the system's high symmetry, the direction of the gradient field can also be changed. As the gradient field in the working area was nearly uniform and only related to the magnitude of the current, it could be expressed as:

$$\boldsymbol{G}_r = i \cdot \hat{G} \cdot \boldsymbol{r} \quad (3)$$

Where $\hat{G}$ represents the unit current gradient field at the center working area and $\boldsymbol{r}$ is the directional vector.

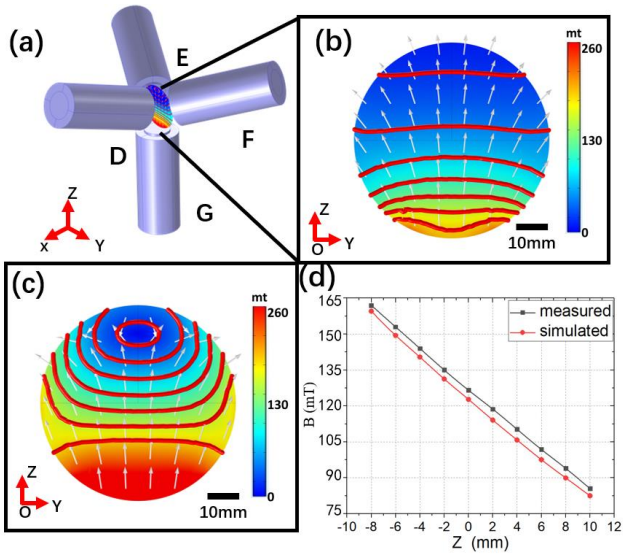

Fig. 2 Simulation of magnetic field. (a) Location of simulated position in the working area (b) Magnetic map generated by electromagnet G at I_G= 15A, I_D= I_E= I_F= 0A (c) Magnetic map resulting from four electromagnets working simultaneously (I_G=15A, I_D= I_E= I_F= -15A) (d) Measured magnetic flux intensity along the Z-axis in the central working area for I_G= 15A, I_D= I_E= I_F= -15A and the gradient reaches up to 4.14T/m.

III. Magnetic Force Modeling

A. Cell-robot culturing

To kill cancer cells, we use macrophage as templates for constructing cell-robots, and it is necessary to address the problem of how to achieve targeted transportation of cells. In fact, magnetic field has good biological penetration and can propel magnetic substance wirelessly. Therefore, we obtained magnetized cell-robots (average diameter = 20 μm) by culturing the mouse macrophages in a medium containing Fe_2O_3 magnetic nanoparticles as shown in Fig. 3.

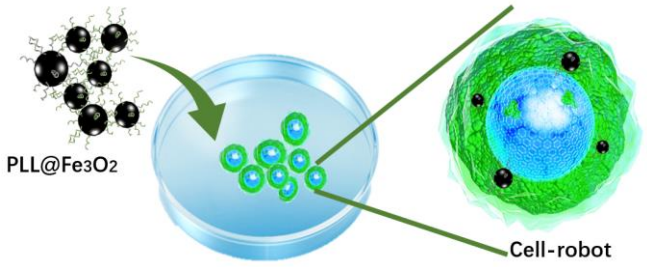

Fig. 3 Schematic of how to manufacture the cell-robots

For the cell-robot, a mouse microphage cell line, RAW264.7, was purchased from the National Infrastructure of Cell Line Resource and maintained in DMEM high glucose supplemented with 10% fetal bovine serum (FBS) (VISTECH, NEW Zealand). The RAW264.7 cells were collected by pipetting from a plate were dissociated using 0.05% trypsin-EDTA (Thermo Fisher Scientific). Then the cells were centrifuged at 2000r/min for 6 min and the resulting pellets were suspended in the growth medium. As for the culture medium, the PLL@Fe_2O_3 nanoparticles were dispersed in an FBS-free DMEM medium (Thermo Fisher Scientific) at a concentration of 25 μg/ml supplemented with citrate at a final concentration of 5 mM to prevent the aggregation of the nanoparticle. Then the cell lines were incubated using the medium in a humid chamber at 37°C and 5% CO_2. Prior to use, the macrophages were incubated in this medium for 24 h, rinsed with DMEM medium, and then returned to a complete proliferation medium containing FBS for at least 2 h. Then, a magnetized cell-robot is obtained as shown in Fig. 4(a). Fig. 4(b) shows the cell-robot captured through a Confocal microscope (FV 3,000, OLYMPUS, Japan), wherein the blue regions are nuclei stained by hoechst33342 while green indicates cytoplasm stained by DIO. The Fe_2O_3 magnetic nanoparticles, which are easily absorbed by macrophages, will impart magnetic characteristics to the cell-robots. Fig. 4(c) displays a cell-robot that has absorbed magnetic nanoparticles, in which the blue regions indicate the magnetic nanoparticles stained by Perls' Prussian blue staining Kit, and it can be seen that there are lots of magnetic particles within the cells which means the cells have already been magnetized.

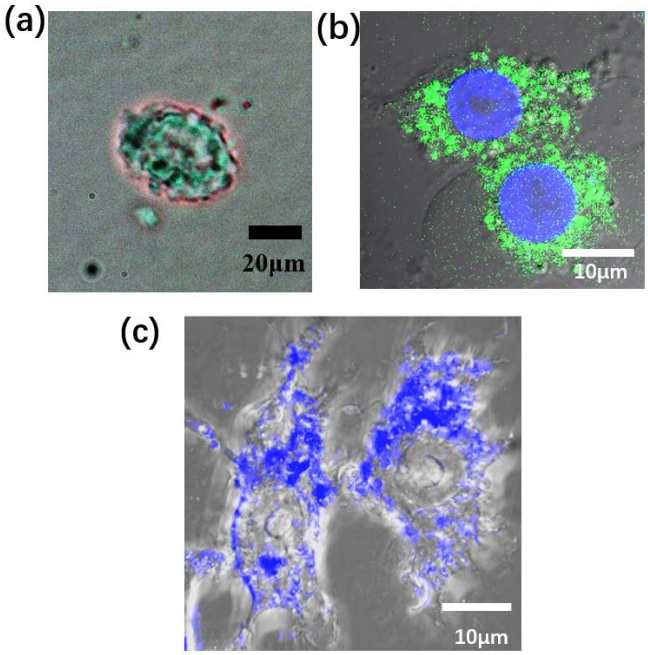

Fig. 4 (a) the cell-robot under optical microscope (b) the magnetized cell-robots: blue regions are nuclei stained by hoechst33342; green indicates cytoplasm stained by DIO. (c) Magnetic particles engulfed by cellular robot: blue indicates stained magnetic nanoparticles by Prussian blue.

B. Magnetic Force propelling the cell-robot

In fact, any magnetic substance in the gradient magnetic field will be subjected to the magnetic force $\boldsymbol{F}$ which will lead to the movement of the magnetic substance. The magnetic force is proportional to the magnetic field gradient G_r and the magnetization vector $\boldsymbol{m}$ of the magnetic material. For the magnetized cell-robot, the magnetic force $\boldsymbol{f}$ can be calculated by the following formula:

$$\boldsymbol{f} = (\boldsymbol{m} \cdot \nabla)\boldsymbol{B} \tag{4}$$

Where m represents the magnetization of the cell-robot, $\nabla = \left[\frac{\partial}{\partial x} \quad \frac{\partial}{\partial y} \quad \frac{\partial}{\partial z}\right]^T$, $\boldsymbol{B} = [B_x \quad B_y \quad B_z]^T$.

As the cell-robot is manufactured based on a mouse macrophage template, its density is close to that of the culture medium, enabling the gravitational and buoyant forces to be offset. Within the magnetic field, the cell-robot is primarily affected by the magnetic force and the resistance of the culture solution. The magnetic force applied to the cellular robot can be calculated from (3) and (4) as:

$$\boldsymbol{F}_{drag} = (\boldsymbol{m}_{cell} \cdot \nabla)\boldsymbol{B} = \boldsymbol{m}_{cell} \cdot G_r \tag{5}$$

where $\boldsymbol{m}_{cell}$ is the magnetization vector of the cell-robot. The resistance of the cell-robot in the medium can be calculated by approximating the robot as a sphere[28]:

$$\boldsymbol{F}_{resistence} = C_D A \frac{\rho \boldsymbol{u}^2}{2} \tag{6}$$

where $A = \pi R^2$ represents the cross-sectional area of the cell-robot, R is its diameter, $\boldsymbol{u}$ is the moving speed, ρ is the density of the solution, and C_D is the drag coefficient, which is related to the diameter of the cell as $C_D = \frac{12\mu}{\rho R u}$, where μ is the kinematic viscosity of the liquid. The viscous resistance can thus be rewritten as:

$$\boldsymbol{F}_{resistence} = 6\pi\mu R\boldsymbol{u}. \tag{7}$$

When the cell-robot moves steadily, the magnetic force on it is equal to the liquid resistance, i.e., $\boldsymbol{F}_{drag} = \boldsymbol{F}_{resistence}$. The magnetization vector of the cell-robot can be calculated by measuring its moving speed.

IV. Experiment and Result

A. Cell-robot control to approach the cancer

For the cancer, the human breast adenocarcinoma cell line MCF-7 was cultured acting as cancer cells, which is very typical. As shown in Fig. 5(a), is the schematic of a cancer cell, while the confocal microscope picture of the cancer cell is shown in Fig. 5(b).

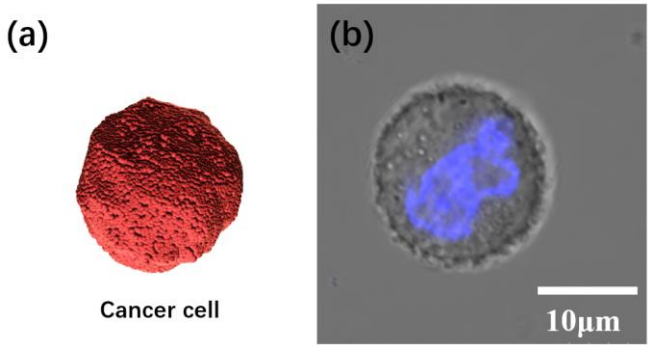

Fig. 5 The cancer cell (a) Schematic diagram of the cancer cell (b) picture of the cancer cell by the confocal microscope: blue indicates nucleus stained by hoechst33342.

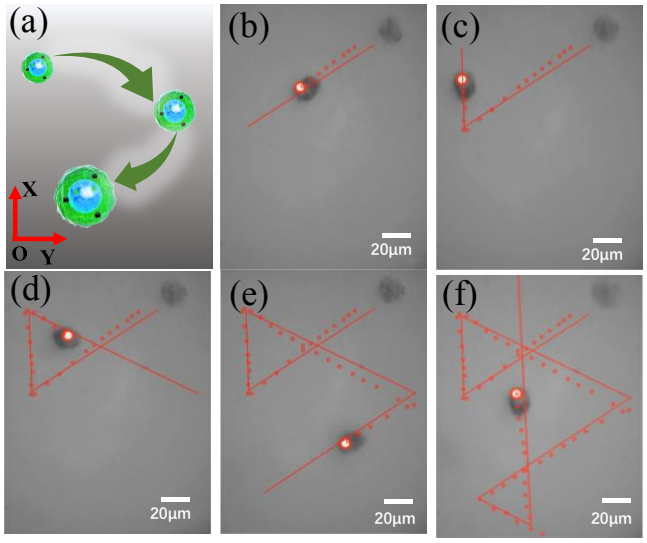

Fig. 6 Process of cell-robot approaching the cancer cell (a) Schematic of the movement of the cell-robot (b)- (f) pictures of cell-robot moving along the planned path. Red solid lines are the planned path and dotted lines are the actual paths.

To kill the cancer cells, it is necessary to control the cell-robot to the destination area. Combined with the established magnetic control system, the complex motion control of the cell-robot can be realized, the diagram is shown in Fig. 6(a). The manipulation of the cell-robot is conducted by the gradient field as simulated in Fig. 2(c). Therefore, the movement of the robot can be realized accurately in vitro and the usage in biomedicine area is promising. As shown in Fig. 6(b)-(f), the manufactured cell-robot is placed in the working place, then the robot is controlled continuously using the gradient field, wherein the red solid lines are the planned path and dotted lines are the actual paths. This means the cell-robot can be propelled by the field for Precision targeted therapy. At this process, the moving speed of the cell-robot is about 9 μm/s, while the gradient field is up to1.68 T/m.

B. Cancer killing process in vitro

Then we transport the cell-robot to the vicinity of the cancer cell. In the initial state, the robot is far away from the cancer cells, therefore it is difficult for the robot to capture the cancer cells automatically. By using the magnetic field, the cell-robot will approach the cancer cells and finally contact the cancer cell, then the cell-robot will begin to phagocytose the cancer cells and eventually kill the cancer cells. In the experiment, we take the same amount of cancer cells and cell-robots and then put them at different side of the dish. Next, the magnetic field is applied to control the cell-robot to move toward the cancer cells. Once the cell-robot moves to the vicinity of the cancer cells, these cells are continuously being cultured. Then at different time period, we took a set of cells, then Calcein-AM (CA) and propidium iodide (PI) Double stain Kit is used to identify if the cells are alive, since the dead cells can be dyed into red while the live cells can be dyed into green as shown in Fig. 7. We found that at different period, the

dead cells varied as the time changes. Fig. 7(a) illustrates the conditions of the initial state while Fig. 7(b) and (c) shows the dead cancer cells after culturing for 6 h and 24 h individually.

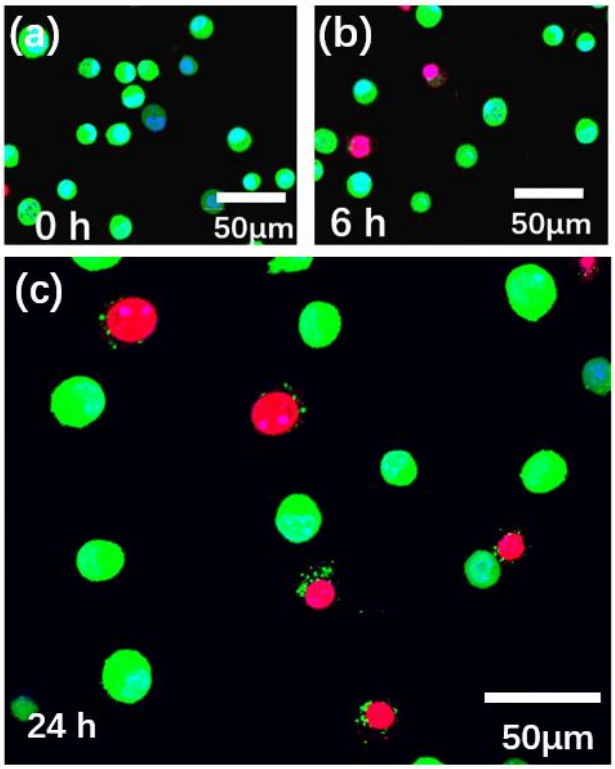

Fig. 7 Results of cell-robot killing cancer cells. Photograph of cancer cells killed by cell-robot at different time periods (Red cells are dead, while green cells are alive) (a) initial state (b) after 6h (c) after 24h

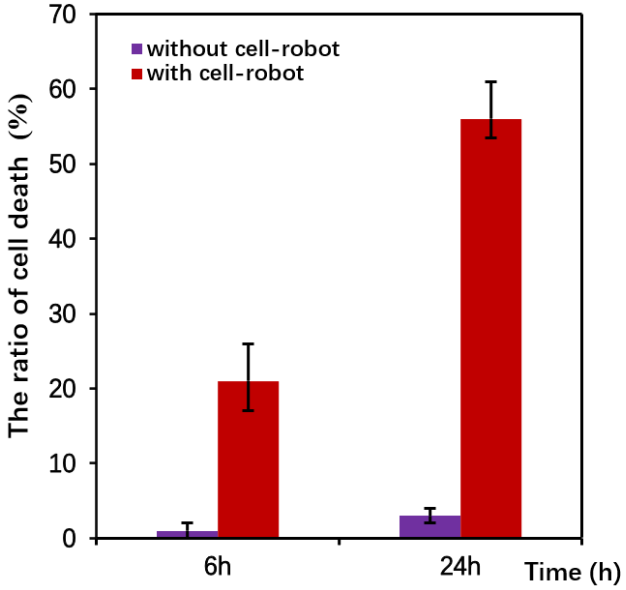

Fig. 8 Proportion of cancer cell death at different time periods.

Considering the effect of the experimental environment, we also conducted the experiments without cell-robots and observe the mortality of cancer cells. It can be found that there is significant difference in the probability of dead cancer cells when the cell-robot are not put it the dish and controlled towards the cancer cell. Still we found that the rate of dead cancel increases as the time goes as shown in Figure 8. Moreover, after 24h, the mortality rate of cancer cells is about 60%, showing great application prospects in biomedicine area, since they are biocompatible and biodegradable.

C. *Cancer killing process in vivo*

To assess the tumor-killing effect of the cell-robots on MCF-7 tumor-bearing mice in vivo, a tumor was planted at the back of the immunocompromised mice. Without any control, the tumor will grow bigger. In the experiment, the cell-robots were then injected into the tail vein of the mice. To observe if the cell-robots can work efficiently, we divided the mice into two groups: the magnet targeted group and non-targeted group. However, to simplify the experiment in vivo, we use a permanent magnet. For the magnet targeted group, a permanent magnet is placed at the tumor area throughout the experiment, while there were no magnets at the non-targeted group. Then the mice of the two groups were raised under the same conditions.

Figure 9 shows the results of the tumor-killing effect of the cell-robot. Fig. 9(a) is the non-targeted group, and it can be seen that the tumor was obvious in 18 days, and the tumor grew much bigger in 30 days. However, in the magnet targeted group as shown in Fig. 9(b), the tumor cannot be found in 18 days. In about 30 days, the tumor grew bigger, but was much smaller compared with the non-targeted group. This verifies that the cell-robots can be controlled by the magnetic field in vivo, and can inhibit the growth of the tumor when injected into the mice.

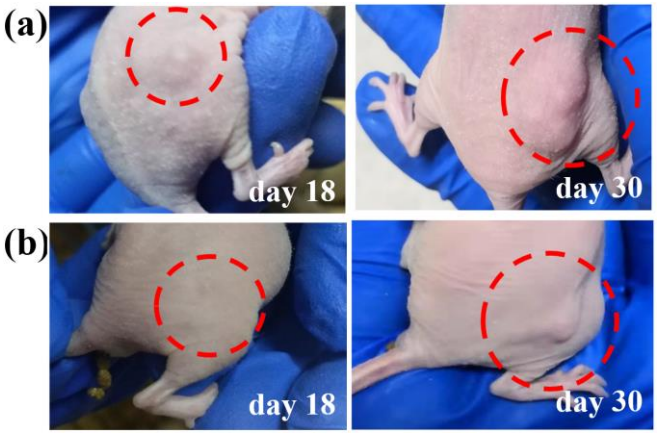

Fig. 9 Results of cell-robot killing tumor in vivo. Area in the red circle is the implanted tumor in mice (a)Photograph of the tumor when the cell-robot is injected into the mice, and a permanent magnet is placed in the tumor area. (b) Photograph of the tumor when there are no permanent magnets placed in the tumor area.

V. Conclusion And Discussions

In this paper, we present a magnetized cell-robot for cancer killing which can be propelled by gradient magnetic field. For that purpose, a magnetic control system is proposed firstly which can generate high gradient field. Then we get the cell-

robot by culturing the mouse macrophages in the culture medium containing Fe_2O_3 magnetic nanoparticles. Human cancer cells are used as abnormal cells which will be detected and eaten by the cell-robots. By using the magnetic field, the cell-robot can be controlled in vitro, and cancer cells can be killed by the cell-robot effectively.

In fact, due to the limited amount of magnetic nanoparticles contained in the cells, a large gradient field is required to drive the cell-robot. At the same time, macrophages are important immune systems in the body. When infected by pathogenic microorganisms, macrophages in the body phagocytose, digest and remove them, not only for cancer cells, but also for various abnormal cells. The cell-robot using macrophages as template is biocompatible and has no degradation problem, which has little harm to the organism. In vivo experiment shows great application prospect in biomedicine in the future.

Future work includes optimizing the control of magnetic fields, establishing vitro vascular models and enabling vitro experiments with cellular robots using the established magnetic system.

REFERENCES

[1] H. W. Tung, M. Maffioli, D. R. Frutiger, K. M. Sivaraman, S. Pane, and B. J. Nelson, "Polymer-Based Wireless Resonant Magnetic Microrobots," *Ieee Transactions on Robotics,* vol. 30, no. 1, pp. 26-32, Feb 2014.

[2] J. F. Yu, B. Wang, X. Z. Du, Q. Q. Wang, and L. Zhang, "Ultra-extensible ribbon-like magnetic microswarm," *Nature Communications,* vol. 9, Aug 21 2018.

[3] L. Feng *et al.*, "On-chip microfluid induced by oscillation of microrobot for noncontact cell transportation," *Applied Physics Letters,* vol. 111, no. 20, Nov 13 2017.

[4] L. Feng, S. Y. Zhang, Y. G. Jiang, D. Y. Zhang, and F. Arai, "Microrobot with passive diamagnetic levitation for microparticle manipulations," *Journal of Applied Physics,* vol. 122, no. 24, Dec 28 2017.

[5] S. E. Chung, X. G. Dong, and M. Sitti, "Three-dimensional heterogeneous assembly of coded microgels using an untethered mobile microgripper," *Lab on a Chip,* vol. 15, no. 7, pp. 1667-1676, 2015.

[6] T. L. Li *et al.*, "Highly Efficient Freestyle Magnetic Nanoswimmer," *Nano Letters,* vol. 17, no. 8, pp. 5092-5098, Aug 2017.

[7] S. Tasoglu, E. Diller, S. Guven, M. Sitti, and U. Demirci, "Untethered micro-robotic coding of three-dimensional material composition," *Nature Communications,* vol. 5, Jan 2014.

[8] Y. Dai, D. Chen, S. Liang, L. Song, Q. Qi, and L. Feng, "A magnetically actuated octopus-like robot capable of moving in 3D space," in *2019 IEEE International Conference on Robotics and Biomimetics (ROBIO)*, 2019, pp. 2201-2206.

[9] I. S. M. Khalil, A. F. Tabak, A. Klingner, and M. Sitti, "Magnetic propulsion of robotic sperms at low-Reynolds number," *Applied Physics Letters,* vol. 109, no. 3, Jul 18 2016.

[10] E. Diller, J. Zhuang, G. Z. Lum, M. R. Edwards, and M. Sitti, "Continuously distributed magnetization profile for millimeter-scale elastomeric undulatory swimming," *Applied Physics Letters,* vol. 104, no. 17, Apr 28 2014.

[11] T. L. Li *et al.*, "Autonomous Collision-Free Navigation of Microvehicles in Complex and Dynamically Changing Environments," *Acs Nano,* vol. 11, no. 9, pp. 9268-9275, Sep 2017.

[12] L. Feng, P. Di, and F. Arai, "High-precision motion of magnetic microrobot with ultrasonic levitation for 3-D rotation of single oocyte," *International Journal of Robotics Research,* vol. 35, no. 12, pp. 1445-1458, Oct 2016.

[13] L. Feng, Y. L. Sun, C. Ohsumi, and F. Arai, "Accurate dispensing system for single oocytes using air ejection," *Biomicrofluidics,* vol. 7, no. 5, Sep 2013.

[14] W. Q. Hu, G. Z. Lum, M. Mastrangeli, and M. Sitti, "Small-scale soft-bodied robot with multimodal locomotion," *Nature,* vol. 554, no. 7690, pp. 81-85, Feb 1 2018.

[15] X. Wang *et al.*, "Facile Fabrication of Magnetic Microrobots Based on Spirulina Templates for Targeted Delivery and Synergistic Chemo-Photothermal Therapy," *Acs Applied Materials & Interfaces,* vol. 11, no. 5, pp. 4745-4756, Feb 6 2019.

[16] M. P. Kummer, J. J. Abbott, B. E. Kratochvil, R. Borer, A. Sengul, and B. J. Nelson, "OctoMag: An Electromagnetic System for 5-DOF Wireless Micromanipulation," *Ieee Transactions on Robotics,* vol. 26, no. 6, pp. 1006-1017, Dec 2010.

[17] A. J. Petruska and B. J. Nelson, "Minimum Bounds on the Number of Electromagnets Required for Remote Magnetic Manipulation," *Ieee Transactions on Robotics,* vol. 31, no. 3, pp. 714-722, Jun 2015.

[18] J. X. Li, B. E. F. de Avila, W. Gao, L. F. Zhang, and J. Wang, "Micro/nanorobots for biomedicine: Delivery, surgery, sensing, and detoxification," *Science Robotics,* vol. 2, no. 4, Mar 15 2017.

[19] X. H. Yan *et al.*, "Magnetite Nanostructured Porous Hollow Helical Microswimmers for Targeted Delivery," *Advanced Functional Materials,* vol. 25, no. 33, pp. 5333-5342, Sep 2015.

[20] J. Y. Li *et al.*, "Development of a magnetic microrobot for carrying and delivering targeted cells," *Science Robotics,* vol. 3, no. 19, Jun 27 2018.

[21] Z. G. Wu *et al.*, "A swarm of slippery micropropellers penetrates the vitreous body of the eye," *Science Advances,* vol. 4, no. 11, Nov 2018.

[22] H. Z. Qi *et al.*, "Blood Exosomes Endowed with Magnetic and Targeting Properties for Cancer Therapy," *Acs Nano,* vol. 10, no. 3, pp. 3323-3333, Mar 2016.

[23] H. Y. Kim *et al.*, "Therapeutic Efficacy-Potentiated and Diseased Organ-Targeting Nanovesicles Derived from Mesenchymal Stem Cells for Spinal Cord Injury Treatment," *Nano Letters,* vol. 18, no. 8, pp. 4965-4975, Aug 2018.

[24] S. J. Madsen, S. K. Baek, A. R. Makkouk, T. Krasieva, and H. Hirschberg, "Macrophages as Cell-Based Delivery Systems for Nanoshells in Photothermal Therapy," *Annals of Biomedical Engineering,* vol. 40, no. 2, pp. 507-515, Feb 2012.

[25] M. Muthana *et al.*, "Directing cell therapy to anatomic target sites in vivo with magnetic resonance targeting," *Nature Communications,* vol. 6, Aug 2015.

[26] T. A. Wynn, A. Chawla, and J. W. Pollard, "Macrophage biology in development, homeostasis and disease," *Nature,* vol. 496, no. 7446, pp. 445-455, Apr 25 2013.

[27] Y. Dai *et al.*, "Untethered Octopus-Inspired Millirobot Actuated by Regular Tetrahedron Arranged Magnetic Field," *Advanced Intelligent Systems,* vol. 2, no. 5, p. 1900148, 2020.

[28] G. K Batchelor, *An Introduction to Fluid Dynamic*. Cambridge University Press, 1967.